Consistent Induction Motor Parameters for the Calculation of Partial Load Efficiencies by Means of an Advanced Simulation Model

C. Kral, A. Haumer, and C. Grabner

***Abstract*—From the rating plate data of an induction motor the nominal efficiency can be determined. Without detailed knowledge of equivalent circuit parameters, partial load behavior cannot be computed. Therefore, a combined calculation and estimation scheme is presented, where the consistent parameters of an equivalent circuit are elaborated, exactly matching the nominal operating point. From these parameters part load efficiencies can be determined.**

***Index Terms*—Induction motor, consistent parameters, partial load efficiency**

I. Introduction

The parameter identification and estimation of permanent magnet or [1], [2] electric excited synchronous motors [3], [4], switched reluctance motors [5], [6] and induction motors [7] is essential for various applications. For a controlled drive the performance is very much related with the accuracy of the determined motor parameters [8]–[20], e.g., in energy efficient drives [21], [22]. Another field of applications which may rely on properly determined parameters is condition monitoring and fault diagnosis of electric motors [23]–[25].

For an induction motor, operated at nominal voltage and frequency, and loaded by nominal mechanical power, the current and power factor indicated on the rating plate show certain deviations of the quantities obtained by measurements. The rating plate data are usually rounded and subject to certain tolerances. Deviations of the measured data from the data stated on the rating plate are therefore not surprising.

For the determination of partial load efficiencies of an induction motor, various methods can be applied. One method would be the direct measurement of the electrical and the mechanical power. A second method applies the principle of loss separation; in this case the power balance according to Fig. 2 can be applied. For this purpose it is also required to identify the required motor parameters.

Under some circumstances, it is demanded to determine the partial load efficiency of an induction motor with little or literally no knowledge about the motor. This is a very challenging task, since the full parameter set of an equivalent circuit cannot be computed consistently from the name plate data without further assumptions or knowledge. Practically, one would identify the parameters of the induction motor through several test methods. Thorough investigations of techniques for the determination of induction motor efficiencies are presented in [26], [27]. In the presented cases the actual efficiency is analyzed more or less independent of the rating plate data.

Manuscript received April 8, 2009.

C. Kral, A. Haumer and C. Grabner are with the Austrian Institute of Technology (AIT), business unit Electric Drive Technologies, Giefinggasse 2, 1210 Vienna, Austria (corresponding author to provide phone: +43(5)0550–6219, fax: +43(5)0550–6595, e-mail: christian.kral@arsenal.ac.at).

In this paper a method for the determination of the consistent parameters of the equivalent circuit of an induction motor is proposed. In this context it is very important to understand, that the proposed approach does not estimate the parameters of a real induction motor. In this sense, consistent parameters mean, that the determined parameters *exactly* model the specified operating point specified by the rating plate data summarized in Tab. I.

Table I
Rating plate data of induction motor

Quantity	Symbol	SI Unit
nominal mechanical output power	$P_{m,N}$	W
nominal phase voltage	$V_{s,N}$	V
nominal phase current	$I_{t,N}$	A
nominal power factor	pf_N	–
nominal frequency	$f_{s,N}$	Hz
nominal speed	n_N	1/s

The estimation of motor parameters from name plate data [28]–[30] is thus not sufficient, since the parameters are not implicitly consistent. This means, that the nominal efficiency computed by means of estimated parameters does *not* exactly compute the nominal operating point.

There are two cases where the determination of consistent parameters is useful. First, a real motor should be investigated, from which, more or less, only the rating plate data are known. Yet partial load efficiencies should be computed for certain operating conditions. Second, the simulation model of an electric drive, which neither has been designed nor built, needs to be parametrized. In such cases, very often only the specification of the nominal operating point is known.

In this paper a calculation for the determination of consistent parameters is proposed. The applied model takes stator and rotor ohmic losses, core losses, friction losses and stray-load losses into account, while exactly modeling the specified nominal operating conditions. Some of the required parameters can either be measured, others may be estimated through growth relationships. Due to implicit consistency restrictions, the remaining parameters are solely determined by mathematical equations.

II. Power and Torque Balance

For the presented power balance and equivalent circuit the following assumptions apply:

- Only three phase induction motors (motor operation) are investigated.
- The motor and the voltage supply are fully symmetrical.
- The voltages and currents are solely steady state and of sinusoidal waveform.
- Only fundamental wave effects of the electromagnetic field are investigated.

- Non-linearities such as saturation and the deep bar effect are not considered.

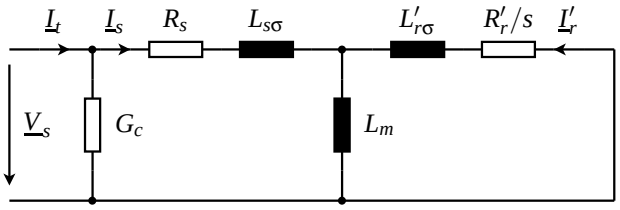

Figure 1. Equivalent circuit of the induction motor

The algorithm presented in this paper relies on the single phase equivalent circuit depicted in Fig. 1. This equivalent circuit considers stator and rotor ohmic losses as well as core losses, which is why the phasors of the terminal current $\underline{I}_t$ and the stator current $\underline{I}_s$ have to be distinguished.

In order to simplify the explicit calculation of the equivalent circuit parameters, the conductor, representing core losses, is connected directly to the stator terminals. In this approach, stator and rotor core losses

$$P_c = 3G_c V_s^2 \tag{1}$$

are modeled together, where G_c represents the total core conductance.

Due to the modeling topology of the equivalent circuit, stator and rotor ohmic losses are

$$P_{\mathrm{Cus}} = 3R_s I_s^2, \tag{2}$$
$$P_{\mathrm{Cur}} = 3R'_r I'^2_r. \tag{3}$$

The rotor parameters of the equivalent circuit are transformed to the stator side, and thus indicated by the superscript $'$.

The inner (electromagnetic) power of the motor is determined by

$$P_i = R'_r \frac{1-s}{s} I'^2_r. \tag{4}$$

Friction and stray-load losses are not considered in the power balance of the equivalent circuit. Nevertheless, these effects have to be taken into account independently.

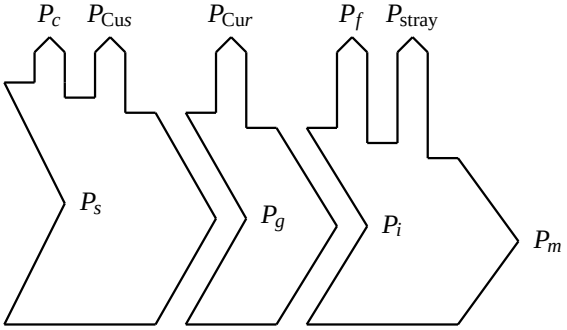

Figure 2. Power balance of the the induction motor

In Fig. 2 the total power balance of the motor is depicted. In this balance, the total electrical input power is P_s, and the air gap power is

$$P_g = P_s - P_c - P_{\mathrm{Cus}}. \tag{5}$$

The inner power

$$P_i = P_g - P_{\mathrm{Cur}} \tag{6}$$

is computed from the inner power and the copper heat losses. Mechanical output (shaft) power

$$P_m = P_i - P_f - P_{\mathrm{stray}} \tag{7}$$

is determined from inner power, P_i, friction losses, P_f, and stray-load losses, P_{stray}.

Instead of the power balance (7) an equivalent torque balance

$$\tau_m = \tau_i - \tau_f - \tau_{\mathrm{stray}}, \tag{8}$$

can be considered. In this context, mechanical output (shaft) torque, τ_m, is associated with the left side of (7), and the inner (electromagnetic) torque, τ_i, is associated with the left side of (6), etc. Each of these torque terms can be multiplied with the mechanical angular rotor velocity Ω_m, to obtain equivalent power terms according to (7).

III. Core, Friction and Stray-Load Losses

A. Core Losses

For the core loss model hysteresis and eddy current losses have to be taken into account [31]. In a certain operating point the total core losses $P_{c,\mathrm{ref}}$ are known. This operating point refers to a reference voltage $V_{s,\mathrm{ref}}$ and the reference frequency $f_{s,\mathrm{ref}}$. Under these conditions a reference conductance can be computed according to

$$G_{c,\mathrm{ref}} = \frac{P_{c,\mathrm{ref}}}{3V^2_{s,\mathrm{ref}}}. \tag{9}$$

The ratio of hysteresis losses with respect to the total core losses – with respect to this reference operating point – is a_h. For any other operating point indicated by the actual phase voltage V_s and frequency f_s, the total core losses can then be expressed by

$$P_c = P_{c,\mathrm{ref}} \left(a_h \frac{f_{s,\mathrm{ref}}}{f_s} \frac{V_s^2}{V^2_{s,\mathrm{ref}}} + (1-a_h) \frac{V_s^2}{V^2_{s,\mathrm{ref}}} \right). \tag{10}$$

>From this relationship the total conductance of the equivalent circuit – as a function of V_s and f_s – can be determined:

$$G_c = G_{c,\mathrm{ref}} \left(a_h \frac{f_{s,\mathrm{ref}}}{f_s} + 1 - a_h \right) \tag{11}$$

Based on the experience of the authors, it is proposed to set $a_h \approx 0.75$, if no other estimation is available. In Fig. 3 the impact of the ratio a_h on the total core losses is depicted. The presented curves are computed for a constant ratio $\frac{V_s}{f_s}$ (in the range $f_s < f_{s,\mathrm{ref}}$) and constant voltage (in the flux weakening range for $f_s \geq f_{s,\mathrm{ref}}$) as depicted in Fig. 4.

B. Friction Losses

The friction losses are modeled by

$$\frac{P_f}{P_{f,\mathrm{ref}}} = \left(\frac{\Omega_m}{\Omega_{m,\mathrm{ref}}} \right)^{a_f+1}, \tag{12}$$

(for $\Omega_m \geq 0$). In this equation $P_{f,\mathrm{ref}}$ and $\Omega_{m,\mathrm{ref}}$ are the friction losses and the mechanical angular rotor velocity with respect to a reference operating point, respectively. For axial or forced ventilation $a_f \approx 1.5$ can be used and radial ventilation can be modeled by $a_f \approx 2$.

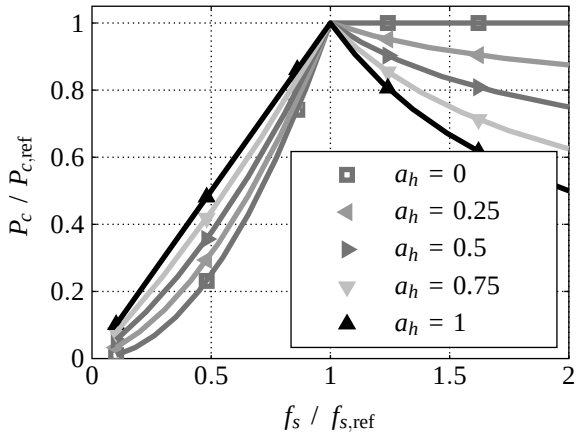

Figure 3. Total core losses versus frequency; constant $\frac{V_s}{f_s}$ for $f_s < f_{s,\mathrm{ref}}$ and constant voltage for $f_s \geq f_{s,\mathrm{ref}}$

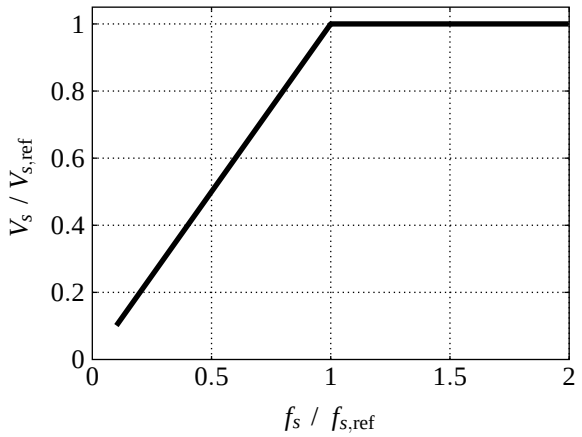

Figure 4. Voltage versus frequency for inverter operation

C. Stray-Load Losses

The stray-load losses are defined as the portion of the total losses in a motor that do not account for stator and rotor ohmic losses, core and friction losses. These losses thus indicate the portion of the losses which can not be calculated. According to the IEEE Standard 112 [32] the percentages a_{stray} of the stray-load losses with respect to the nominal output power for the nominal operating point are summarized in Tab. II.

Table II
STRAY-LOAD PERCENTAGES ACCORDING TO IEEE STANDARD 112

nominal output power [kW]	percentage a_{stray}
1–90	0.018
91–375	0.015
376–1850	0.012
greater than 1850	0.009

>From the actual terminal current I_t and the no load terminal current $I_{t,0}$, the approximated rotor current can be calculated by

$$I_2 = \sqrt{I_t^2 - I_{t,0}^2}. \tag{13}$$

In the IEEE Standard 112, the stray-load losses are considered by a quadratic dependency of (13). Since the standard does not take any variable frequency dependencies into account, the stray-load loss are proposed to be approximated by

$$P_{\mathrm{stray}} = a_{\mathrm{stray}} P_{m,N} \frac{I_t^2 - I_{t,0}^2}{I_{t,N}^2 - I_{t,0}^2} \left(\frac{\Omega_m}{\Omega_{m,N}} \right)^2, \tag{14}$$

which can be considered as an extension to the standard [33]. In [34], the stray-load losses are considered as an equivalent resistor in the equivalent circuit. Since the voltage drop across such a resistor has no physical background, the stray-load losses are modeled differently in this paper: the stray-load losses are inherently taken into account by an equivalent breaking torque,

$$\tau_{\mathrm{stray}} = a_{\mathrm{stray}} P_{m,N} \frac{I_t^2 - I_{t,0}^2}{I_{t,N}^2 - I_{t,0}^2} \frac{\Omega_m}{\Omega_{m,N}^2}, \tag{15}$$

according to (8).

IV. SPACE PHASOR EQUATIONS

The space phasor equations of electric machines can be derived based on the definitions of [35]. With respect to the equivalent circuit of Fig. 1, the stator voltage and terminal current space phasor (with respect to the stator fixed reference) frame are

$$\underline{V}_s^s = \frac{2}{3}(v_{s,1} + e^{\mathrm{j}2\pi/3} v_{s,2} + e^{-\mathrm{j}2\pi/3} v_{s,3}), \tag{16}$$

$$\underline{I}_t^s = \frac{2}{3}(i_{t,1} + e^{\mathrm{j}2\pi/3} i_{t,2} + e^{-\mathrm{j}2\pi/3} i_{t,3}), \tag{17}$$

where $v_{s,1}$, $v_{s,2}$ and $v_{s,3}$ are the stator phase voltages, and $i_{t,1}$, $i_{t,2}$ and $i_{t,3}$ are the terminal phase currents, respectively. These space phasors can be transformed into a synchronous reference frame; the angular velocity of this reference frame is

$$\omega_s = 2\pi f_s. \tag{18}$$

The reference frame of the transformed stator voltage and terminal current is indicated by a superscript index:

$$\underline{V}_s^f = \underline{V}_s^s e^{-\mathrm{j}(\omega_s t - \varphi_f)} \tag{19}$$

$$\underline{I}_t^f = \underline{I}_t^s e^{-\mathrm{j}(\omega_s t - \varphi_f)} \tag{20}$$

The electrical rotor speed is

$$\omega_m = p\Omega_m, \tag{21}$$

since space phasor theory relies on an equivalent two pole induction motor. The voltage equations with respect to Fig. 1 are

$$\begin{bmatrix} \underline{V}_s^f \\ 0 \\ \underline{V}_s^f \end{bmatrix} = \begin{bmatrix} 0 & R_s + \mathrm{j}\omega_s L_s & \mathrm{j}\omega_s L_m \\ 0 & \mathrm{j}\omega_r L_m & R_r + \mathrm{j}\omega_r L_r \\ 1/G_c & -1/G_c & 0 \end{bmatrix} \begin{bmatrix} \underline{I}_t^f \\ \underline{I}_s^f \\ \underline{I}_r^f \end{bmatrix}, \tag{22}$$

where

$$\omega_r = \omega_s - \omega_m. \tag{23}$$

The rotor leakage and main field inductances of the equivalent circuit in Fig. 1 and the rotor resistance cannot be determined independently [36]. It is thus useful to introduce the stray factor

$$\sigma = 1 - \frac{L_m^2}{L_s L_r'}, \tag{24}$$

and the ratio of stator to rotor inductance

$$\sigma_{sr} = \frac{L_s}{L_r'}, \tag{25}$$

as well as the terms

$$a_s = \frac{\omega_s L_s}{R_s}, \tag{26}$$

$$a_r = \frac{\omega_r L_r'}{R_r'}. \tag{27}$$

The linear set of equations (22) has the solutions

$$\underline{I}_s^f = \underline{V}_s^f \frac{a_s(1+\mathrm{j}a_r)}{\omega_s L_s[1-\sigma a_s a_r+\mathrm{j}(a_s+a_r)]}, \quad (28)$$

$$\underline{I}_r^f = \underline{V}_s^f \frac{-\mathrm{j}\sqrt{1-\sigma}\sqrt{\sigma_{sr}}a_s a_r}{\omega_s L_s[1-\sigma a_s a_r+\mathrm{j}(a_s+a_r)]}, \quad (29)$$

according to [37]. The inner torque yields:

$$\tau_i = \frac{3p}{2}\frac{V_s^2}{\omega_s^2 L_s}\frac{(1-\sigma)a_s^2 a_r}{(1-\sigma a_s a_r)^2+(a_s+a_r)^2} \quad (30)$$

It is obvious that (28) and (30) are independent of σ_{sr}. This is an important result, which refutes the myth that for a squirrel cage induction motor the inductance L_r' can be determined without further assumptions. Yet, the rotor current (29) is certainly dependent on σ_{sr}. For the assignment of specific values to the parameters L_m, L_r' and R_r' and for the calculation of the rotor current the arbitrary factor σ_{sr} has to be chosen according to

$$1-\sigma \le \sigma_{sr} \le \frac{1}{1-\sigma}. \quad (31)$$

V. Determination of Parameters

In the following a combination of parameter calculations and estimations, based on empirical data, is presented. The presented results all refer to empirical data obtained from 50 Hz standard motors. Unfortunately the empiric data cannot be revealed in this paper. Nevertheless the applied mathematical approach for the estimation is presented. For motors with a certain mechanical power and number of pole pairs empirical data can be approximated with good accuracy.

The determination of the equivalent circuit parameters is, however, based on the rating plate data of the motor (Tab. I). From these data the nominal electrical input power

$$P_{s,N} = 3V_{s,N}I_{t,N}\,\mathrm{pf}_N \quad (32)$$

and the nominal angular rotor velocity

$$\Omega_{m,N} = 2\pi n_N \quad (33)$$

can be computed.

A. Measurement or Estimation of Core Losses

If measurement results are obtained from a real motor, the core losses can be determined according to IEEE Standard 122 [32], by separating core and friction losses. The no load core losses, $P_{c,0}$, refer to the nominal voltage and nominal frequency. It is assumed that the no load test is performed at synchronous speed ($s=0$),

$$\Omega_{m,0} = \frac{2\pi f_{s,N}}{p}. \quad (34)$$

In case measurement results are not available, the no load friction losses, for a motor with a certain nominal mechanical output power, $P_{m,N}$, and a certain number of pole pairs, p, can be estimated from empirical data by

$$\log_{10}\left(\frac{P_{c,0}}{P_c'}\right) = k_{c[p]}\log_{10}\left(\frac{P_{m,N}}{P_m'}\right) + d_{c[p]}. \quad (35)$$

In this equation, P_c' and P_m' are arbitrary reference power terms to normalize the argument of the logarithm. The parameters $k_{c[p]}$ and $d_{c[p]}$ are obtained from the empiric data and particularly refer to a specific number of pole pairs. From the estimated or measured no load core losses the reference core conductance can be derived according to (9),

$$G_{c,\mathrm{ref}} = \frac{P_{c,0}}{3V_{s,N}}. \quad (36)$$

B. Measurement or Estimation of Friction Losses

>From a no load test ($s=0$) the friction losses, $P_{f,0}$, of a particular real motor can also be determined. In case no measurements are available, the no load friction losses can be estimated from empirical data,

$$\log_{10}\left(\frac{P_{f,0}}{P_f'}\right) = k_{f[p]}\log_{10}\left(\frac{P_{m,N}}{P_m'}\right) + d_{f[p]}. \quad (37)$$

In this equation P_f' and P_m' are some arbitrary reference power terms, and $k_{f[p]}$ and $d_{f[p]}$ are empiric parameters corresponding for a certain number of pole pairs. According to (12), the no load friction losses $P_{f,0} = P_{f,\mathrm{ref}}$ are corresponding with $\Omega_{m,0} = \Omega_{m,\mathrm{ref}}$.

C. Calculation of Stray-Load Losses

The nominal stray load losses can be derived from

$$P_{\mathrm{stray},N} = a_{\mathrm{stray}}P_{m,N}, \quad (38)$$

and parameter a_{stray} can be obtained by Tab. II.

D. Estimation of Stator Resistance

The stator resistance can be estimated applying the power balance of Fig. 2 with respect to the nominal operation point. From the nominal mechanical output power, $P_{m,N}$, the nominal friction losses

$$P_{f,N} = P_{f,0}\left(\frac{\Omega_{m,N}}{\Omega_{m,0}}\right)^{a_f+1} \quad (39)$$

and the nominal stray-load losses (38), the nominal inner power

$$P_{i,N} = P_{m,N} - P_{f,N} - P_{\mathrm{stray},N} \quad (40)$$

can be calculated. The air gap power can be determined from the nominal inner power and nominal slip, s_N [37]:

$$P_{g,N} = \frac{P_{i,N}}{1-s_N} \quad (41)$$

The stator copper losses can then be obtained by the power balance (5), applied to the nominal operating point,

$$P_{\mathrm{Cus},N} = P_{s,N} - P_{g,N} - P_{c,N}. \quad (42)$$

Since the core loss conductor is connected to the terminals in Fig. 1, the core losses with respect to the nominal and no load operating point are equal,

$$P_{c,N} = P_{c,0}. \quad (43)$$

>From the the nominal stator phase current, and the nominal stator copper losses (42) consistent stator resistance are determined by

$$R_s = \frac{P_{\mathrm{Cu},s,N}}{3I_{s,N}^2}. \quad (44)$$

In this equation the nominal stator current, $I_{s,N}$ has to be determined from (22).

Alternatively to this approach the stator resistance can be measured or estimated. The core losses (43) can then be

derived through a numeric iteration. In other words: there are two options on how the stator resistance and the core losses can be determined. Either the stator resistance or the core losses have to be measured or estimated, and the remaining quantity can then be computed by (40)–(44).

E. Measurement or Estimation of No Load Current

In the following space phasor calculations are applied to the nominal operating conditions. The phase angle φ_f of synchronous reference is chosen such way that the imaginary part of the stator voltage space phasor

$$\underline{V}^f_{s,N} = V_{sx,N} + \mathrm{j}V_{sy,N} \tag{45}$$

is zero,

$$V_{sx,N} = \sqrt{2}V_{s,N} \tag{46}$$
$$V_{sy,N} = 0. \tag{47}$$

If the no load terminal current

$$\underline{I}^f_{t,0} = I_{tx,0} + \mathrm{j}I_{ty,0} \tag{48}$$

has not been obtained by measurement results, the reactive component has to be estimated. This can be performed by

$$\log_{10}\left(\frac{I_{ty,0}}{I'_{ty,0}}\right) = k_{0[p]}\log_{10}\left(\frac{P_{m,N}}{P'_m}\right) + d_{0[p]}, \tag{49}$$

where $I'_{ty,0}$ and P'_m are an arbitrary reference current and power term. The parameters $k_{0[p]}$ and $d_{0[p]}$ are estimated from empiric data with respect to a certain number of pole pairs. Then the imaginary part of the stator current space phasor can be derived by

$$I_{sy,0} = I_{ty,0}, \tag{50}$$

according to (48) and (22). Once all the parameters of the motor are determined, the consistent no load current $I_{t,0}$ can be determined from the equivalent circuit, evaluating (14).

F. Determination of Stator Inductance

The rotor current space phasor diminishes under no load conditions, and thus the stator current equation of (22) yields:

$$\sqrt{2}V_{s,N} = R_s I_{sx,0} - \omega_s L_s I_{yx,0} \tag{51}$$
$$0 = \omega_s L_s I_{sx,0} + R_s I_{sy,0} \tag{52}$$

By eliminating the real part, $I_{sx,0}$, in these equations, the remaining equation for the imaginary part, considering $I_{sy,0} < 0$, can be used to determine the stator inductance

$$L_s = -\frac{V_{sx,N} + \sqrt{V^2_{sx,N} - 4R^2_s I^2_{sy,0}}}{2\omega_s I_{sy,0}}. \tag{53}$$

G. Determination of Stray Factor and Rotor Time Constant

The components of the nominal terminal current space phasor are

$$\underline{I}^f_{t,N} = I_{tx,N} + \mathrm{j}I_{ty,N} \tag{54}$$

>From the components of the terminal current

$$I_{tx,N} = +I_{t,N}\,\mathrm{pf}_N, \tag{55}$$
$$I_{ty,N} = -I_{t,N}\sqrt{1-\mathrm{pf}^2_N}, \tag{56}$$

the components of the stator current space phasor can be derived:

$$I_{sx,N} = I_{tx,N} - \sqrt{2}G_c V_{s,N}, \tag{57}$$
$$I_{sy,N} = I_{ty,N}. \tag{58}$$

The real and the imaginary part of (28) yields:

$$\frac{V_{sx,N}}{R_s} = (1-\sigma a_s a_r)I_{sx,N} - (a_s + a_r)I_{sy,N} \tag{59}$$
$$\frac{a_r}{a_s}\frac{V_{sx,N}}{R_s} = (a_s + a_r)I_{sx,N} + (1-\sigma a_s a_r)I_{sy,N} \tag{60}$$

>From these two equations the two unknown parameters

$$a_r = \frac{a_s R_s I^2_{s,N} + I_{sy,N}V_{sx,N}}{I_{sx,N}V_{sx,N} - R_s I^2_{s,N}}, \tag{61}$$

$$\sigma = \frac{(2I_{sx,N} - a_s I_{sy,N})V_{sx,N} - R_s I^2_{s,N} - \frac{V^2_{sx,N}}{R_s}}{a_s(a_s R_s I^2_{s,N} + I_{sy,N}V_{sx,N})}, \tag{62}$$

can be obtained. The rotor time constant is the ratio of the rotor inductance and the rotor resistance and can be expressed in terms of known parameters, utilizing (27),

$$T_r = \frac{a_r}{\omega_{r,N}}, \tag{63}$$

where $\omega_{r,N}$ refers to the nominal operating point. From (61)–(63) it can be seen that the rotor time constant and the leakage factor are independent of the particular choice of σ_{sr}.

H. Determining Magnetizing Inductance, Rotor Inductance and Rotor Resistance

>From the leakage factors σ and σ_{sr}, and the stator inductance L_s, utilizing (31), the following equations can be derived:

$$L_m = L_s\frac{\sqrt{1-\sigma}}{\sqrt{\sigma_{sr}}} \tag{64}$$
$$L'_r = \frac{L_s}{\sigma_{sr}} \tag{65}$$

>From (63) and (65) the rotor resistance can be computed.

$$R'_r = \frac{L'_r}{T_r}. \tag{66}$$

The quantities determined in this subsection are fully dependent on the particular choice of σ_{sr}.

VI. Advanced Simulation Model

For the numerical investigation of the machine a numerical simulation model can be used. Such an advanced simulations model is presented in this section.

The squirrel cage of an induction machine can be seen as a multiphase winding with shorted turns. Instead of a wound structure the rotor consists of N_r bars and two end rings, connecting the bars on both ends, as depicted in Fig. 5 and 6. At the end rings fins are located to force the circulation of air in the inner region of the machine.

The presented machine topology is modeled in *Modelica*, an acausal object oriented modeling language for multi physical systems [38]. In the *Modelica Standard Library* (MSL) a standard set of physical packages for electric, mechanic, thermal, control and logic components is collected. The *Machines* package provides models of electric machines based on text book equations. The modeled three phase induction machines

rely on space phasor theory and a full symmetry of the stator and rotor winding. Electrical rotor asymmetries can therefore not be modeled using the MSL.

In order to model electrical rotor asymmetries the full topology of the rotor cage, respectively has to be taken into account. Such models are developed in the *ExtendedMachines* Library [39].

Figure 5. Scheme of a rotor cage of an induction machine

Figure 6. Rotor cage of an induction machine

A. Model of Stator Winding

It is assumed in the following that the stator winding is fully symmetrical. Additionally, the number of stator phases is restricted to three. In this case the stator voltage equation can be written as

$$V_{s[i]} = R_s I_{s[i]} + L_{s\sigma}\frac{\mathrm{d}I_{s[i]}}{\mathrm{d}t} + \sum_{j=1}^{3} L_{sm[i,j]}\frac{\mathrm{d}I_{s[j]}}{\mathrm{d}t} + \sum_{j=1}^{N_r}\frac{\mathrm{d}L_{sr[i,j]}I_{r[j]}}{\mathrm{d}t}, \quad (67)$$

where $V_{s[i]}$ and $I_{s[i]}$ and $I_{r[i]}$ are the stator voltages and stator currents and the rotor currents, respectively. The stator resistance R_s and the stator stray inductance $L_{s\sigma}$ are symmetrical, due to the symmetry of the stator winding. The coupling of the stator windings is represented by the main field inductance matrix

$$L_{sm[i,j]} = L_0 w_s^2 \xi_s^2 \cos\left[\frac{(i-j)2\pi}{3}\right]. \quad (68)$$

The mutual coupling between the stator and rotor is represented by the matrix

$$L_{sr[i,j]} = L_0 w \xi_s \xi_r \cos\left[\frac{(i-1)2\pi}{3} - \frac{(j-1)2\pi}{N_r} - \gamma_m\right]. \quad (69)$$

Both these matrices are fully symmetrical, since it is assumed that the coupling over the magnetic main field is not influenced by the any electric asymmetry. The term L_0 indicates the base inductance of a coil without chording, i.e., the coil width equal to the pole pitch. The number of series connected turns and the winding factor of the stator winding are represented by the parameters w_s and ξ_s. The product $w_s\xi_s$ is thus the *effective number of turns*. The winding factor of the rotor winding

$$\xi_r = \sin\left(\frac{p\pi}{N_r}\right) \quad (70)$$

is a pure geometric factor, which is derived from the mesh width of two adjacent rotor bars [40]. In this equation, however, skewing is not considered [41]. The quantity γ_m represents the electric displacement angle of the rotor with respect to the stator.

The effective number of turns, $w_s\xi_s$, can be determined from a winding topology, which is indicated by the begin and end location and the number of turns of the stator winding coils – as depicted in Fig. 7. Alternatively, a symmetric stator winding may be parametrized by entering the effective number of turns.

B. Model of Rotor Winding

The winding topology of the squirrel cage rotor with N_r rotor bars can be seen as a winding with an effective number of turns equal to one. The matrix of the main rotor field can be expressed as

$$L_{rr[i,j]} = L_0 \xi_r^2 \cos\left[\frac{(i-j)2\pi}{N_r}\right]. \quad (71)$$

For the bars and the end rings on both sides (index a = drive end side, DE; index b = non drive end, NDE) constant leakage inductances $L_{b[i]}$ and $L_{ea[i]}$ and $L_{eb[i]}$ are considered. The rotor voltage equations can be derived form the equivalent circuit of a rotor mesh as shown in Fig. 8:

$$\begin{aligned} 0 \;=\; & (R_{ea[i]} + R_{eb[i]} + R_{b[i]} + R_{b[i+1]})I_{r[i]} \\ & - R_{b[i]}I_{r[i-1]} - R_{b[i+1]}I_{r[i]} + R_{eb[i]}I_{eb} \\ & + (L_{ea[i]} + L_{eb[i]} + L_{b[i]} + L_{b[i+1]})\frac{\mathrm{d}I_{r[i]}}{\mathrm{d}t} \\ & - \frac{\mathrm{d}}{\mathrm{d}t}(L_{b[i]}I_{r[i-1]} + L_{b[i+1]}I_{r[i]} - L_{eb[i]}I_{eb}) \\ & + \sum_{j=1}^{3}\frac{\mathrm{d}L_{sr[j,i]}I_{s[j]}}{\mathrm{d}t} + \sum L_{rr[i,j]}\frac{\mathrm{d}I_{r[j]}}{\mathrm{d}t} \end{aligned} \quad (72)$$

In this equation $R_{b[i]}$ are the bar resistances, and $R_{ea[i]}$ and $R_{eb[i]}$ are the resistances of the end ring segments on both sides. Due to the topology of the rotor cage (Fig. 6), $N_r + 1$ linearly independent meshes have to be taken into account. The mesh current I_{eb} is thus introduced and the additional voltage equation

$$0 = \sum_{i=1}^{N_r} R_{eb[i]}(I_{r[i]} + I_{eb}) + \frac{\mathrm{d}}{\mathrm{d}t}\sum_{i=1}^{N_r} L_{eb[i]}(I_{r[i]} + I_{eb}) \quad (73)$$

has to be considered, accordingly.

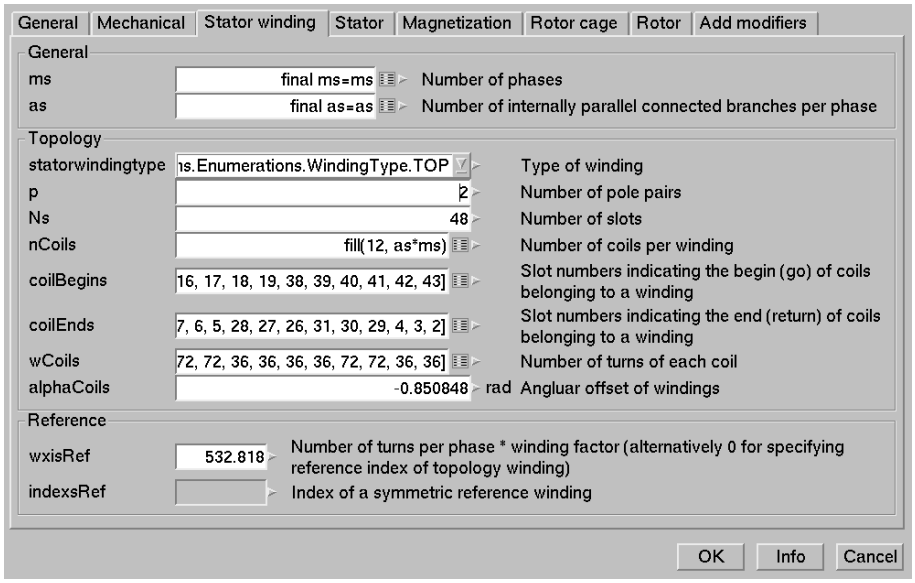

Figure 7. Example of parameters of the stator winding of a squirrel cage induction machine

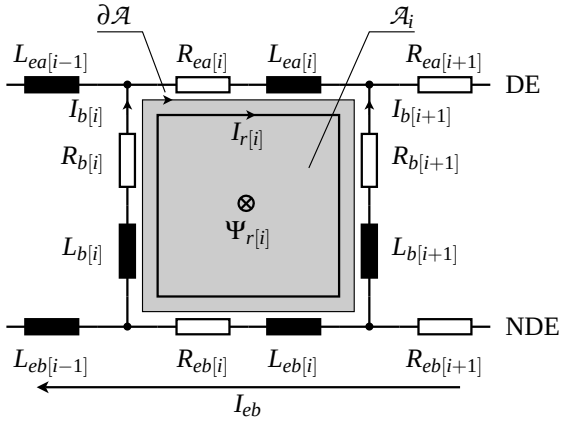

Figure 8. Rotor cage topology (DE = drive end, NDE = non drive end)

As the air gap of the induction machine is modeled with smooth surface, the main field inductances $L_{ss[i,j]}$ and $L_{rr[i,j]}$ are constant and only the mutual inductances (69) are a function of the rotor angle γ_m.

The rotor cage can be parametrized in the *ExtendedMachines* library in two different ways. First, a symmetric rotor cage can be indicated by the rotor resistance R'_r and the rotor leakage inductance $L'_{r\sigma}$, equivalently transformed to the stator side. These are the typical parameters as they appear in the an equivalent circuit of the induction machine. The same parameters are also used for the Machines package of the MSL. Second, each resistance and leakage inductance of the rotor bars and the end ring segments on both sides can be parametrized (Fig. 6) – which is how the squirrel cage modeled internally. The relationship between the symmetric rotor bar and end ring resistance and the rotor resistance with respect to the stator side is determined by

$$R'_r = 2\frac{3{w_s}^2{\xi_s}^2}{N_r{\xi_r}^2}\{R_{e,\mathrm{sym}} + R_{b,\mathrm{sym}}[1-\cos(\frac{2\pi p}{N_r})]\}, \qquad (74)$$

where p is the number of pole pairs. A similar equation can be obtained for the rotor leakage inductance with respect to the stator side,

$$L'_{r\sigma} = 2\frac{3{w_s}^2{\xi_s}^2}{N_r{\xi_r}^2}\{L_{e\sigma,\mathrm{sym}} + L_{b\sigma,\mathrm{sym}}[1-\cos(\frac{2\pi p}{N_r})]\}. \qquad (75)$$

For the symmetric cage the ratios of the resistances, ρ_r, and leakage inductances, ρ_l, each with respect to the rotor bars over the end ring segments, can be specified,

$$\rho_r = \frac{R_{b,\mathrm{sym}}}{R_{e,\mathrm{sym}}}, \qquad (76)$$

$$\rho_l = \frac{L_{b\sigma,\mathrm{sym}}}{L_{e\sigma,\mathrm{sym}}}. \qquad (77)$$

This way, the symmetric cage resistance and leakage inductance parameters can be determined from R'_r, $L'_{r\sigma}$, ρ_r (`ratioCageR` in Fig. 10) and ρ_l (`ratioCageL` in Fig. 10).

Table III
RATING PLATE OF 18.5 KW MOTOR

Quantity	Value
nominal mechanical output power	$P_{m,N} = 18.5\,\mathrm{kW}$
nominal phase voltage	$V_{s,N} = 400\,\mathrm{V}$
nominal phase current	$I_{t,N} = 18.9\,\mathrm{A}$
nominal power factor	$\mathrm{pf}_N = 0.9$
nominal frequency	$f_{s,N} = 50\,\mathrm{Hz}$
nominal speed	$n_N = 1460\,\mathrm{rpm}$

Table IV
PARAMETERS OF 18.5 KW MOTOR

Parameter	Value
stator resistance	$R_s = 0.4784\,\Omega$
stator inductance	$L_s = 0.2755\,\mathrm{H}$
stray factor	$\sigma = 0.05683$
magnetizing inductance	$L_m = 0.2676\,\mathrm{H}$
rotor inductance	$L_r = 0.2755\,\mathrm{H}$
rotor resistance	$R_r = 0.5625\,\Omega$
core conductance	$G_{c,0} = 0.0007539\,\mathrm{S}$
no load friction losses	$P_{f,0} = 211.4\,\mathrm{W}$
nominal stray-load losses	$P_{\mathrm{stray},N} = 333.0\,\mathrm{W}$

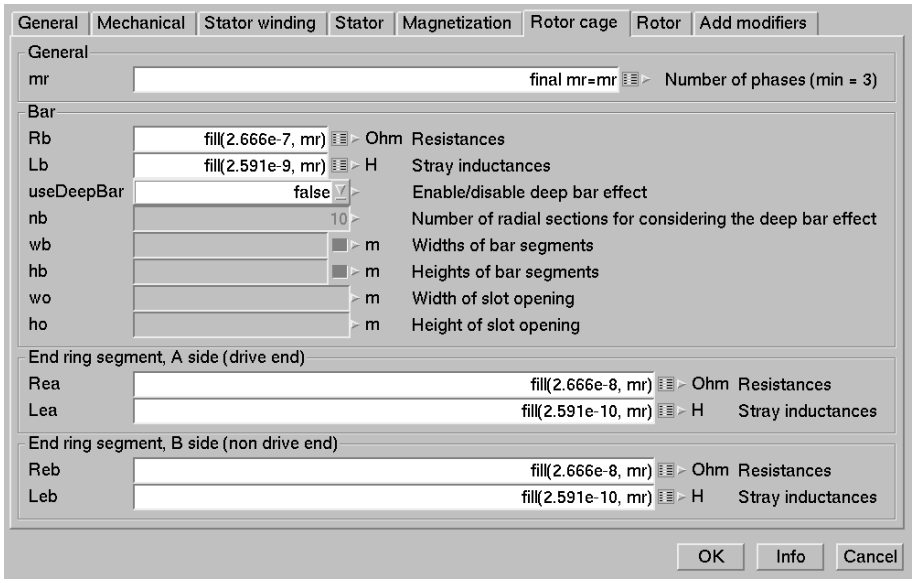

Figure 9. Example of parameters of the resistances and the leakage inductances of the rotor bars and end ring segments

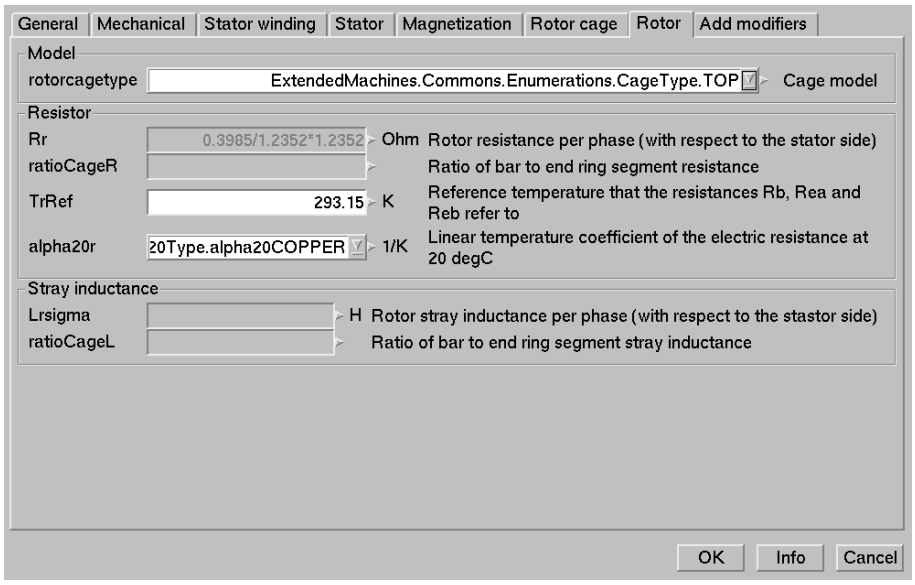

Figure 10. Example of parameters of the squirrel cage

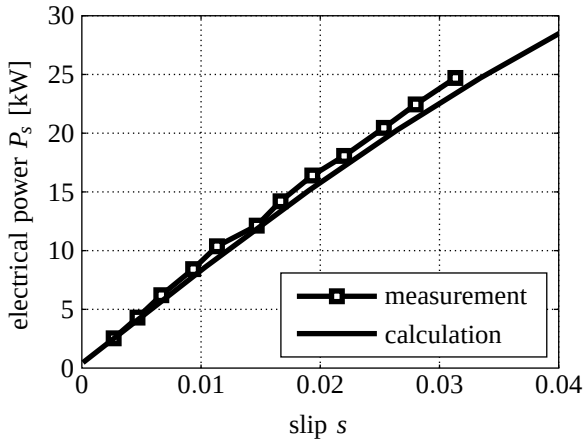

Figure 12. Electrical input power versus slip of a four pole induction motor with 18.5kW; measurement and calculation

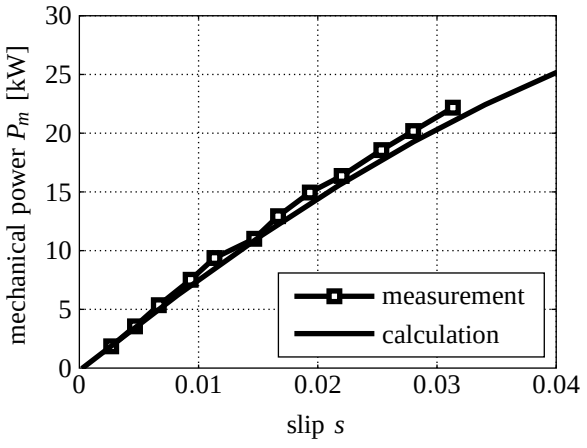

Figure 13. Mechanical output power versus slip of a four pole induction motor with 18.5kW; measurement and calculation

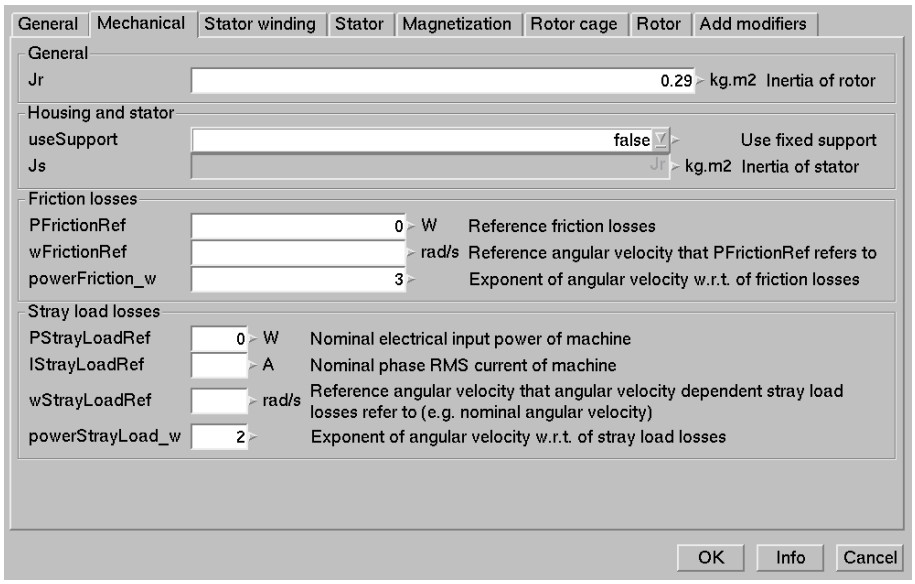

Figure 11. Example of parameters of friction and stray load losses

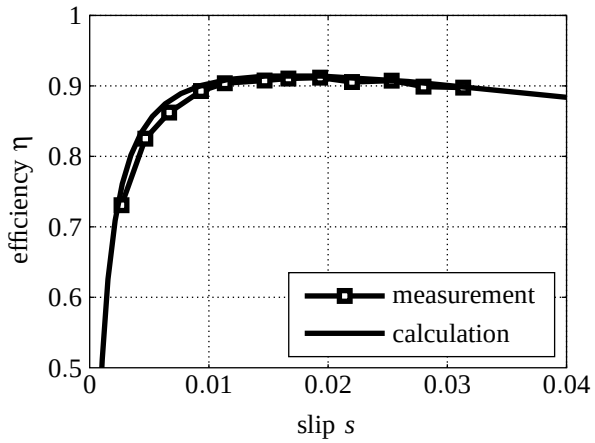

Figure 14. Efficiency versus slip of a four pole induction motor with 18.5kW; measurement and calculation

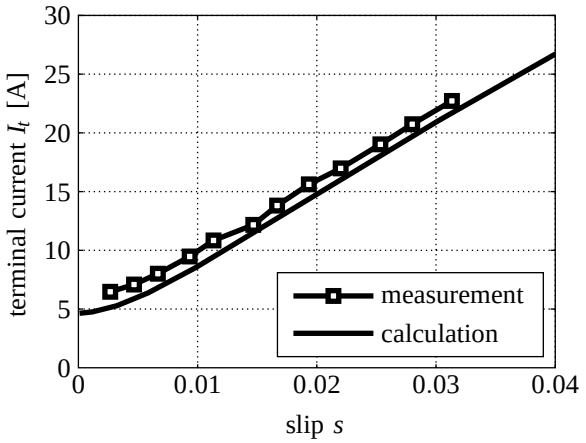

Figure 16. Terminal current versus slip of a four pole induction motor with 18.5kW; measurement and calculation

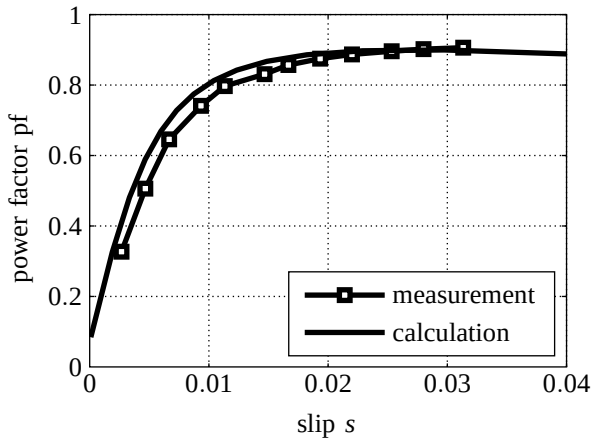

Figure 15. Power factor versus slip of a four pole induction motor with 18.5kW; measurement and calculation

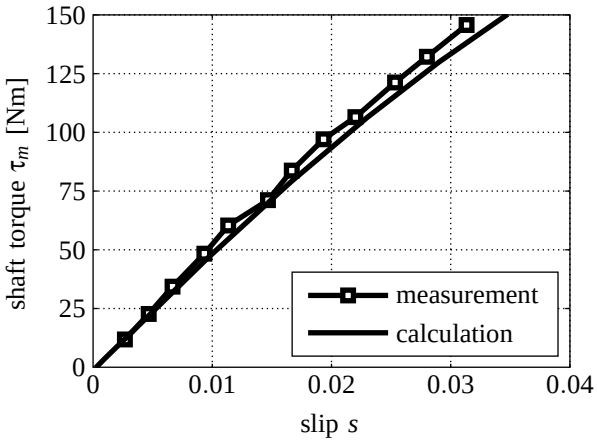

Figure 17. Mechanical output torque versus slip of a four pole induction motor with 18.5kW; measurement and calculation

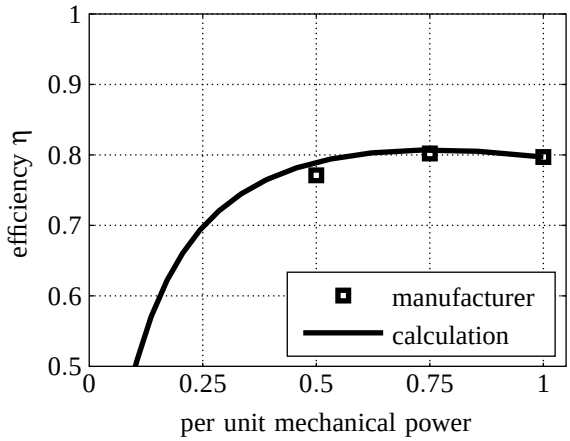

Figure 18. Efficiency versus per unit mechanical output power for a two pole induction motor with $P_{m,N} = 1.1\,\text{kW}$, $V_{s,N} = 400\,\text{V}$, $I_{s,N} = 1.34\,\text{A}$, $\text{pf}_N = 0.86$, $f_{s,N} = 50\,\text{Hz}$ and $n_N = 2810\,\text{rpm}$; manufacturer data and calculation

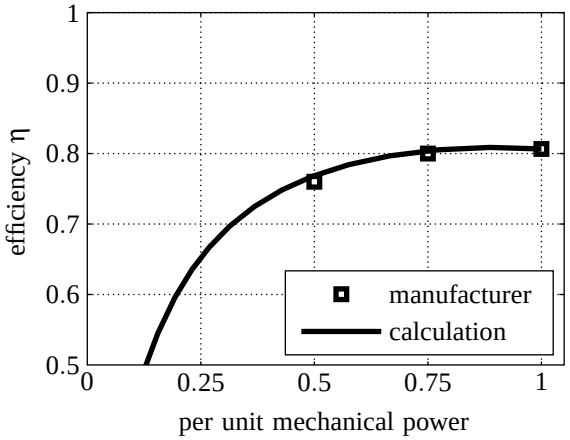

Figure 19. Efficiency versus per unit mechanical output power for a four pole induction motor with $P_{m,N} = 1.1\,\text{kW}$, $V_{s,N} = 400\,\text{V}$, $I_{s,N} = 1.48\,\text{A}$, $\text{pf}_N = 0.769$, $f_{s,N} = 50\,\text{Hz}$ and $n_N = 1446\,\text{rpm}$; manufacturer data and calculation

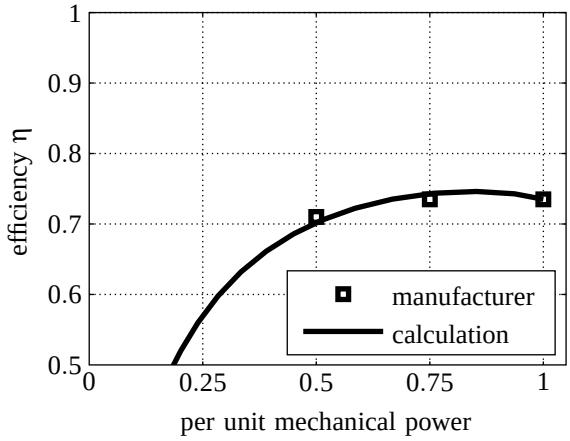

Figure 20. Efficiency versus per unit mechanical output power for a six pole induction motor with $P_{m,N} = 1.1\,\text{kW}$, $V_{s,N} = 400\,\text{V}$, $I_{s,N} = 1.66\,\text{A}$, $\text{pf}_N = 0.75$, $f_{s,N} = 50\,\text{Hz}$ and $n_N = 918\,\text{rpm}$; manufacturer data and calculation

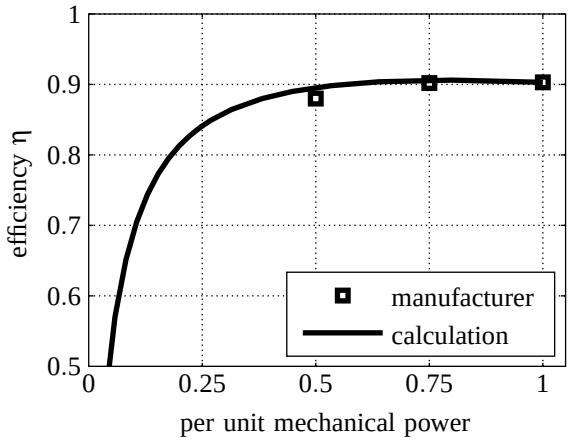

Figure 21. Efficiency versus per unit mechanical output power for a two pole induction motor with $P_{m,N} = 11\,\text{kW}$, $V_{s,N} = 400\,\text{V}$, $I_{s,N} = 11.4\,\text{A}$, $\text{pf}_N = 0.89$, $f_{s,N} = 50\,\text{Hz}$ and $n_N = 2967\,\text{rpm}$; manufacturer data and calculation

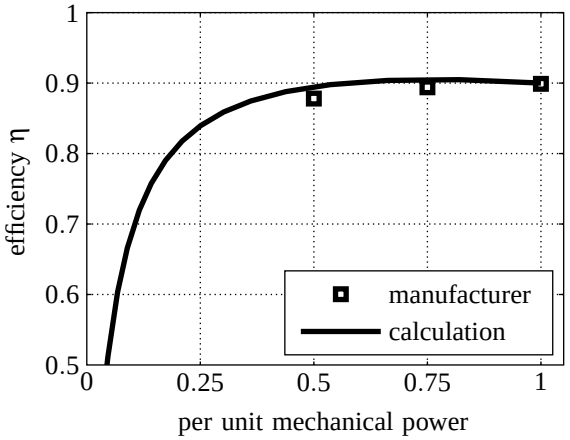

Figure 22. Efficiency versus per unit mechanical output power for a four pole induction motor with $P_{m,N} = 11\,\text{kW}$, $V_{s,N} = 400\,\text{V}$, $I_{s,N} = 12.1\,\text{A}$, $\text{pf}_N = 0.84$, $f_{s,N} = 50\,\text{Hz}$ and $n_N = 1488\,\text{rpm}$; manufacturer data and calculation

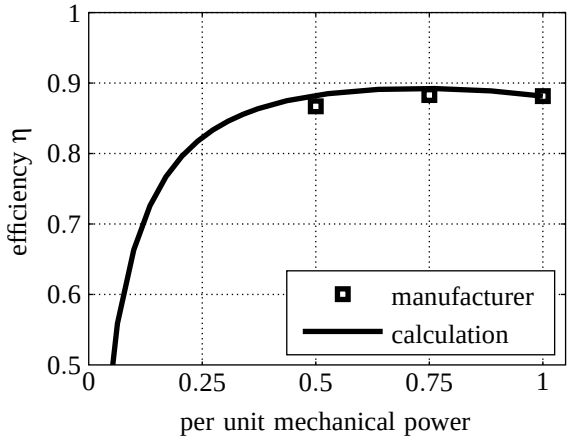

Figure 23. Efficiency versus per unit mechanical output power for a six pole induction motor with $P_{m,N} = 11\,\text{kW}$, $V_{s,N} = 400\,\text{V}$, $I_{s,N} = 13.2\,\text{A}$, $\text{pf}_N = 0.79$, $f_{s,N} = 50\,\text{Hz}$ and $n_N = 876\,\text{rpm}$

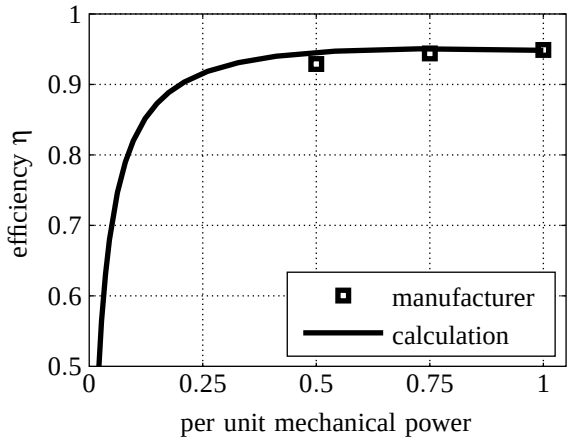

Figure 24. Efficiency versus per unit mechanical output power for a two pole induction motor with $P_{m,N} = 110\,\text{kW}$, $V_{s,N} = 400\,\text{V}$, $I_{s,N} = 107\,\text{A}$, $\text{pf}_N = 0.90$, $f_{s,N} = 50\,\text{Hz}$ and $n_N = 2976\,\text{rpm}$; manufacturer data and calculation

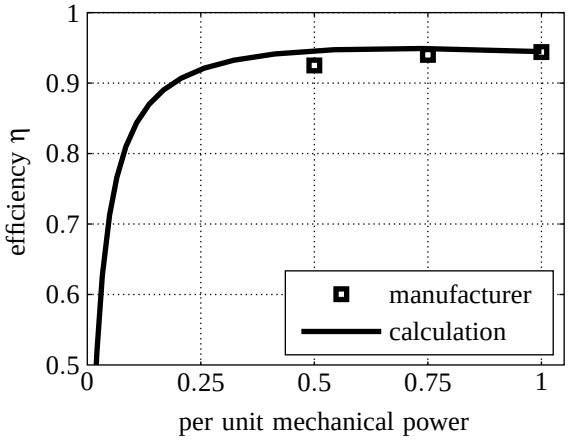

Figure 25. Efficiency versus per unit mechanical output power for a four pole induction motor with $P_{m,N} = 110\,\text{kW}$, $V_{s,N} = 400\,\text{V}$, $I_{s,N} = 110.3\,\text{A}$, $\text{pf}_N = 0.88$, $f_{s,N} = 50\,\text{Hz}$ and $n_N = 1485\,\text{rpm}$; manufacturer data and calculation

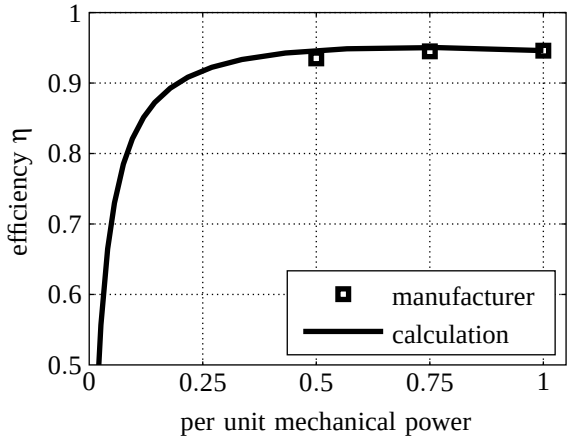

Figure 26. Efficiency versus per unit mechanical output power for a six pole induction motor with $P_{m,N} = 110\,\text{kW}$, $V_{s,N} = 400\,\text{V}$, $I_{s,N} = 116\,\text{A}$, $\text{pf}_N = 0.84$, $f_{s,N} = 50\,\text{Hz}$ and $n_N = 985\,\text{rpm}$; manufacturer data and calculation

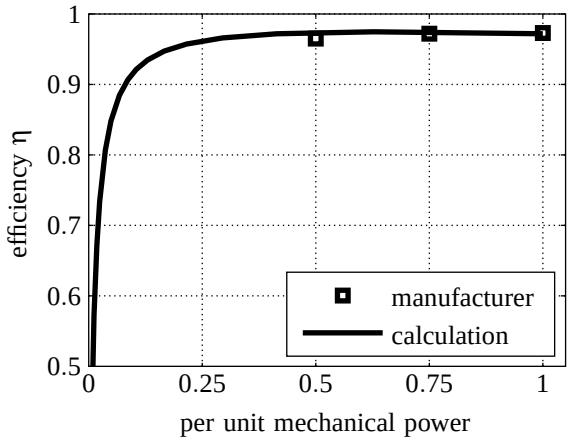

Figure 27. Efficiency versus per unit mechanical output power a for two pole induction motor with $P_{m,N} = 1000\,\text{kW}$, $V_{s,N} = 3464\,\text{V}$, $I_{s,N} = 109\,\text{A}$, $\text{pf}_N = 0.91$, $f_{s,N} = 50\,\text{Hz}$ and $n_N = 2988\,\text{rpm}$; manufacturer data and calculation

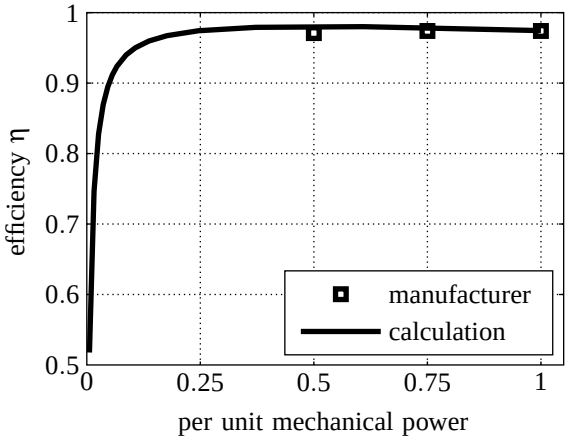

Figure 28. Efficiency versus per unit mechanical output power for a four pole induction motor with $P_{m,N} = 1000\,\text{kW}$, $V_{s,N} = 3464\,\text{V}$, $I_{s,N} = 114\,\text{A}$, $\text{pf}_N = 0.87$, $f_{s,N} = 50\,\text{Hz}$ and $n_N = 1494\,\text{rpm}$; manufacturer data and calculation

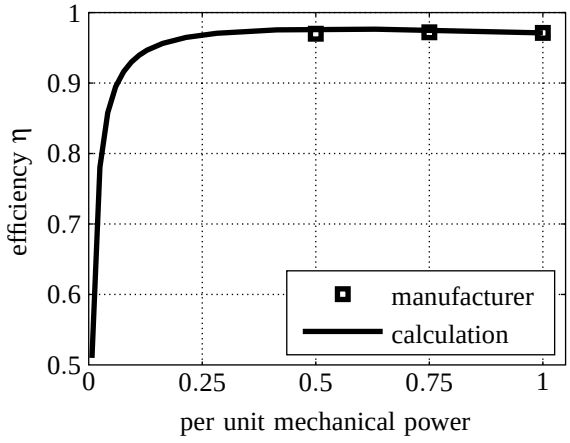

Figure 29. Efficiency versus per unit mechanical output power for a six pole induction motor with $P_{m,N} = 1000\,\text{kW}$, $V_{s,N} = 3464\,\text{V}$, $I_{s,N} = 113\,\text{A}$, $\text{pf}_N = 0.88$, $f_{s,N} = 50\,\text{Hz}$ and $n_N = 996\,\text{rpm}$; manufacturer data and calculation

C. Torque Equation

The inner electromagnetic torque of the machine is determined by

$$T_{\mathrm{el}} = \sum_{i=1}^{3} \sum_{j=1}^{N_r} \frac{\mathrm{d}L_{sr[i,j]}}{\mathrm{d}\gamma_m} I_{s[i]} I_{r[j]}, \tag{78}$$

where $\frac{\mathrm{d}L_{sr[i,j]}}{\mathrm{d}\gamma_m}$ can be expressed analytically from (69). Even if friction, ventilation losses and stray load losses are also taken into account according to section III (Fig. 11).

VII. Measurement and Calculation Results

Table V
Calculated power and losses for nominal operation of 18.5 kW motor

parameter	value
electrical input power	$P_{s,N} = 20412\,\mathrm{W}$
core losses	$P_{c,N} = 361.9\,\mathrm{W}$
stator ohmic losses	$P_{\mathrm{Cus},N} = 498.1\,\mathrm{W}$
rotor ohmic losses	$P_{\mathrm{Cur},N} = 521.4\,\mathrm{W}$
friction losses	$P_{f,N} = 197.6\,\mathrm{W}$
stray-load losses	$P_{\mathrm{stray},N} = 333.0\,\mathrm{W}$
mechanical output power	$P_{m,N} = 18500\,\mathrm{W}$

A. Investigation of a 18.5 kW Motor

A detailed comparison of calculation and measurement results is presented for a 18.5 kW four pole induction motor. In Tab. III the rating plate data of the induction motor are summarized. The investigations are performed for the motor operated at nominal voltage and frequency. Core and friction losses are known from a no load test. The stray load losses are determined according to Tab. II. For this motor the consistent parameters are calculated and summarized in Tab. IV with $\sigma_{sr} = 1$, $a_h = 0.75$, $a_f = 1.5$, and $a_{\mathrm{stray}} = 0.018$. The losses corresponding with the nominal operating point are calculated (Tab. V).

In Fig. 12 and 13 the measurement and calculation results of the electrical input and the mechanical output power are compared. The efficiency

$$\eta = \frac{P_m}{P_s} \tag{79}$$

and the power factor are depicted in Fig. 14 and 15. The stator current and the mechanical output torque are shown in Fig. 16 and 17. The validity and usability of the proposed calculation algorithm is demonstrated by the presented measurement and calculation results.

Since the computation of the consistent parameters is based on the rating plate data of the motor, it is not surprising that the nominal operating point (specified by the rating plate) and the measurement results do not exactly coincide. Instead, a higher goal is achieved: the calculations exactly match the specified nominal operating point.

B. Investigation of Motors based on Manufacturer Data

The series of 1.1 kW, 11 kW, 110 kW and 1000 kW induction motors is also investigated in this paper. For each power rating, manufacturer data of motors for $p = 1$, $p = 2$ and $p = 3$ are compared with calculations (and estimations, respectively). Apart from the nominal operating point, manufacturer data provide additionally the efficiencies for 75% and 50% of the nominal mechanical output power. In Fig. 18–29 the catalog based manufacturer data and the results obtained from calculations are compared.

VIII. Conclusions

The intention of this paper was the calculation of the consistent parameters of an induction motor. In this context it is important to know that the proposed approach does not model the real motor behavior, but exactly models the nominal operating point, specified by the rating plate. In the presented model ohmic losses, core losses, friction losses and stray-load losses are considered. Mathematical algorithms and estimations – where necessary – are presented. For an investigated four pole 18.5 kW induction motor, measurement and calculation results are compared, revealing well matching results and thus proving the applicability of the presented calculations. Additionally, the manufacturer data of a series of two, four and six pole motors in the range of 1.1 kW to 1000 kW are compared with calculations. Even for these motors the obtained manufacturer data show that the calculations are very well matching.

Appendix

Nomenclature

Variables

a	abbreviation; factor
d	term of approximation
φ	phase angle
G	reluctance
i	instantaneous current
I	RMS current
$\underline{I}$	current phasor
k	term of approximation
L	inductance
p	number of pole pairs
P	power, losses
pf	power factor
Ψ	flux linkage
$\underline{\Psi}$	flux linkage phasor
R	resistance
σ	leakage factor
s	slip
T	time constant
τ	torque
v	instantaneous voltage
V	RMS voltage
$\underline{V}$	voltage phasor
ω	electrical angular velocity
Ω	mechanical angular velocity

Indexes

0	no load operation
1,2,3	phase indexes
c	core
Cu	copper
e	eddy current losses
f	friction losses
g	air gap
h	hysteresis losses
i	inner
m	magnetizing; mechanical (rotor)
N	nominal operation

r	rotor
s	stator
sr	stator and rotor
stray	stray-load losses
t	terminal
x	real part, with respect to a synchronous reference frame
y	imaginary part, with respect to a synchronous reference frame

Superscripts

f	synchronous reference frame
s	stator fixed reference frame
$*$	conjugate complex
$'$	with respect to the stator side; reference

REFERENCES

[1] J.-Y. Lee, S.-H. Lee, G.-H. Lee, J.-P. Hong, and J. Hur, "Determination of parameters considering magnetic nonlinearity in an interior permanent magnet synchronous motor," *IEEE Transactions on Magnetics*, vol. 42, pp. 1303–1306, April 2006.

[2] M. Kondo, "Parameter measurements for permanent magnet synchronous machines," *Transactions on Electrical and Electronic Engineering IEEJ Trans 2007*, vol. 109-117, 2007.

[3] M. Burth, G. C. Verghese, and M. Velez-Reyes, "Subset selection for improved parameter estiamtion on on-line identification on a synchronous generator," *IEEE Transactions on Power Systems*, vol. 14, no. 1, pp. 218–225, 1999.

[4] E. Kyriakides, G. Heydt, and V. Vittal, "Online parameter estimation of round rotor synchronous generators including magnetic saturation," *IEEE Transactions on Energy Conversion*, vol. 20, pp. 529–537, Sept. 2005.

[5] S. Ichikawa, M. Tomita, S. Doki, and S. Okuma, "Sensorless control of synchronous reluctance motors based on extended emf models considering magnetic saturation with online parameter identification," *IEEE Transactions on Industry Applications*, vol. 42, pp. 1264–1274, Sept.-Oct. 2006.

[6] P. Niazi and H. A. Toliyat, "Online parameter estimation of permanent-magnet assisted synchronous reluctance motor," *IEEE Transactions on Industry Applications*, vol. 43, pp. 609–615, March-april 2007.

[7] R. Babau, I. Boldea, T. J. E. Miller, and N. Muntean, "Complete parameter identification of large induction machines from no-load acceleration–deceleration tests," *IEEE Transactions on Industrial Electronics*, vol. 54, pp. 1962–1972, Aug. 2007.

[8] R. F. F. Koning, C. T. Chou, M. H. G. Verhaegen, J. B. Klaassens, and J. R. Uittenbogaart, "A novel approach on parameter identification for inverter driven induction machines," *IEEE Transactions on Control Systems Technology*, vol. 8, 6, pp. 873–882, 2000.

[9] J.-K. Seok and S.-K. Sul, "Induction motor parameter tuning for high-performance drives," *IEEE Transactions on Industry Applications*, vol. 37, no. 1, pp. 35–41, 2001.

[10] H. Tajima, G. Guidi, and H. Umida, "Consideration about problems and solutions of speed estimation method and parameter tuning for speed-sensorless vector control of induction motor drives," *IEEE Transactions on Industry Applications*, vol. 38, No. 5, pp. 1282–1289, 2002.

[11] C. Grantham and D. J. McKinnon, "Rapid parameter determination for induction motor analysis and control," *IEEE Transactions on Industry Applications*, vol. 39, pp. 1014–1020, July-August 2003.

[12] R. Wamkeue, I. Kamwa, and M. Chacha, "Unbalanced transients-based maximum likelihood identification of induction machine parameters," *IEEE Transactions on Energy Conversion*, vol. 18, pp. 33–40, March 2003.

[13] H. A. Toliyat, E. Levi, and M. Raina, "A review of rfo induction motor parameter estimation techniques," *IEEE Transactions on Energy Conversion*, vol. 18, pp. 271–283, June 2003.

[14] M. Cirrincione, M. Pucci, G. Cirrincione, and G.-A. Capolino, "A new experimental application of least-squares techniques for the estimation of the induction motor parameters," *IEEE Transactions on Industry Applications*, vol. 39, No. 5, pp. 1247–1256, 2003.

[15] M. Cirrincione, M. Pucci, G. Cirrincione, and G.-A. Capolino, "Constrained minimization for parameter estimation of induction motors in saturated and unsaturated conditions," *IEEE Transactions on Industrial Electronics*, vol. 52, pp. 1391–1402, Oct. 2005.

[16] A. Boglietti, A. Cavagnino, and M. Lazzari, "Experimental high-frequency parameter identification of ac electrical motors," *IEEE Transactions on Industry Applications*, vol. 43, pp. 23–29, Jan.-feb. 2007.

[17] H. Kobayashi, S. Katsura, and K. Ohnishi, "An analysis of parameter variations of disturbance observer for motion control," *IEEE Transactions on Industrial Electronics*, vol. 54, pp. 3413–3421, Dec. 2007.

[18] A. B. Proca and A. Keyhani, "Sliding-mode flux observer with online rotor parameter estimation for induction motors," *IEEE Transactions on Industrial Electronics*, vol. 54, pp. 716–723, April 2007.

[19] D. P. Marcetic and S. N. Vukosavic, "Speed-sensorless ac drives with the rotor time constant parameter update," *IEEE Transactions on Industrial Electronics*, vol. 54, pp. 2618–2625, Oct. 2007.

[20] S. Maiti, C. Chakraborty, Y. Hori, and M. C. Ta, "Model reference adaptive controller-based rotor resistance and speed estimation techniques for vector controlled induction motor drive utilizing reactive power," *IEEE Transactions on Industrial Electronics*, vol. 55, pp. 594–601, Feb. 2008.

[21] A. Mirecki, X. Roboam, and F. Richardeau, "Architecture complexity and energy efficiency of small wind turbines," *IEEE Transactions on Industrial Electronics*, vol. 54, pp. 660–670, Feb. 2007.

[22] D. de Almeida Souza, W. C. P. de Aragao Filho, and G. C. D. Sousa, "Adaptive fuzzy controller for efficiency optimization of induction motors," *IEEE Transactions on Industrial Electronics*, vol. 54, pp. 2157–2164, Aug. 2007.

[23] X.-Q. Liu, H.-Y. Zhang, J. Liu, and J. Yang, "Fault detection and diagnosis of permanent-magnet dc motor based on parameter estimation and neural network," *IEEE Transactions on Industrial Electronics*, vol. 47, pp. 1021–1030, Oct. 2000.

[24] C. Kral, R. Wieser, F. Pirker, and M. Schagginger, "Sequences of field-oriented control for the detection of faulty rotor bars in induction machines—the vienna monitoring method," *IEEE Transactions on Industrial Electronics*, vol. 47, pp. 1042–1050, October 2000.

[25] S. Bachir, S. Tnani, J. C. Trigeassou, and G. Champenois, "Diagnosis by parameter estimation of stator and rotor faults occurring in induction machines," *IEEE Transactions on Industrial Electronics*, vol. 53, pp. 963–973, June 2006.

[26] J. Hsu, J. Kueck, M. Olszewski, D. Casada, P. Otaduy, and L. Tolbert, "Comparison of induction motor field efficiency evaluation methods," *IEEE Transactions on Industry Applications*, vol. 34, pp. 117–125, Jan.-Feb. 1998.

[27] B. Lu, T. Habetler, and R. Harley, "A survey of efficiency-estimation methods for in-service induction motors," *IEEE Transactions on Industry Applications*, vol. 42, pp. 924–933, July-August 2006.

[28] H. König, "Ermittlung der Parameter der Drehstrom-Asynchronmaschine vorwiegend aus den Typenschildangaben," *Elektrie*, vol. 6, pp. 220–220, 1988.

[29] J. Pedra and F. Corcoles, "Estimation of induction motor double-cage model parameters from manufacturer data," *IEEE Transactions on Energy Conversion*, vol. 19, pp. 310–317, June 2004.

[30] K. Davey, "Predicting induction motor circuit parameters," *IEEE Transactions on Magnetics*, vol. 38, pp. 1774–1779, July 2002.

[31] D. Lin, P. Zhou, W. Fu, Z. Badics, and Z. Cendes, "A dynamic core loss model for soft ferromagnetic and power ferrite materials in transient finite element analysis," *Conference Proceedings COMPUMAG*, 2003.

[32] IEEE, "Standard test procedures for polyphase induction motors and generators," *IEEE Standard 112*, 2004.

[33] W. Lang, *Über die Bemessung verlustarmer Asynchronmotoren mit Käfigläufer für Pulsumrichterspeisung*. PhD thesis, Technische Universität Wien, 1984.

[34] P. Pillay, V. Levin, P. Otaduy, and J. Kueck, "In-situ induction motor efficiency determination using the genetic algorithm," *IEEE Transactions on Energy Conversion*, vol. 13, pp. 326–333, Dec. 1998.

[35] P. K. Kovacs, *Transient Phenomena in Electrical Machines*. Budapest: Akademiai Kiado Verlag, 1984.

[36] H. Kleinrath, "Ersatzschaltbilder für Transformatoren und Asynchronmaschinen," *e&i*, vol. 110, pp. 68–74, 1993.

[37] H. Jordan, V. Klima, and K. P. Kovacs, *Asynchronmaschinen*. Braunschweig: F. Vieweg & Sohn Verlag, 1975.

[38] P. Fritzson, *Principles of Object-Oriented Modeling and Simulation with Modelica 2.1*. Piscataway, NJ: IEEE Press, 2004.

[39] C. Kral, A. Haumer, and F. Pirker, "A modelica library for the simulation of electrical asymmetries in multiphase machines - the extended machines library," *IEEE International Symposium on Diagnostics for Electric Machines, Power Electronics and Drives, The 6th, SDEMPED 2007, Cracow, Poland*, pp. 255–260, 2007.

[40] C. Kral, *Modellbildung und Betriebsverhalten einer Asynchronmaschine mit defektem Rotorstab im Läuferkäfig einschließlich Detektion durch die Vienna Monitoring Method*. PhD thesis, Technische Universität Wien, 1999.

[41] G. Müller, *Elektrische Maschinen - Theorie rotierender elektrischer Maschinen*. Berlin: VEB Verlag Technik, 2 ed., 1967.